

**$^{13}\text{C}$  NMR line-shape studies of the organic superconductor  $\kappa\text{-(ET)}_2\text{Cu}[\text{N}(\text{CN})_2]\text{Br}$** 

S. M. De Soto and C. P. Slichter

*Department of Physics and Materials Research Laboratory, University of Illinois at Urbana-Champaign, 1110 West Green Street, Urbana, Illinois 61801-3080*

A. M. Kini, H. H. Wang, U. Geiser, and J. M. Williams

*Chemistry and Materials Science Division, Argonne National Laboratory, Argonne, Illinois 60439*

(Received 22 January 1996)

The authors report  $^{13}\text{C}$  NMR line position, line shape, and spin-spin relaxation rate data for the quasi-two-dimensional organic superconductor  $\kappa\text{-(ET)}_2\text{Cu}[\text{N}(\text{CN})_2]\text{Br}$  ( $T_c = 11.6$  K), for an aligned single crystal. The data make possible identification of the crystallographic site responsible for the NMR lines, clarify a line broadening transition near 150 K, and probe the nature of the fluxoid lattice below  $T_c$ .  
[S0163-1829(96)05246-0]

**I. INTRODUCTION**

Charge-transfer salts based on the BEDT-TTF (hereafter ET) molecule display a variety of ground-state phenomena, including superconductivity and weak ferromagnetism. The ET-based organic superconductor with the highest superconducting transition temperature at ambient pressure is  $\kappa\text{-(ET)}_2\text{Cu}[\text{N}(\text{CN})_2]\text{Br}$  ( $T_c = 11.6$  K). This salt has a layered structure and quasi-two-dimensional (2D) electronic conduction, and experimentally has much in common with the high- $T_c$  superconductors.

We have used  $^{13}\text{C}$  NMR to extend our study of the normal and superconducting states of  $\kappa\text{-(ET)}_2\text{Cu}[\text{N}(\text{CN})_2]\text{Br}$ . In our earlier paper<sup>1</sup> and also in the works of Mayaffre *et al.*<sup>2</sup> and Kawamoto *et al.*,<sup>3</sup> it was demonstrated that the temperature dependence of the spin-lattice relaxation rate indicates that the normal state is not that of a simple metal; instead, strong antiferromagnetic (AF) correlations are present. The AF order found in  $\kappa\text{-(ET)}_2\text{Cu}[\text{N}(\text{CN})_2]\text{Br}$  is not surprising because the isostructural salt  $\kappa\text{-(ET)}_2\text{Cu}[\text{N}(\text{CN})_2]\text{Cl}$  also has strong AF correlations and actually undergoes a transition to an insulating magnetic state near 27 K. In the superconducting state of  $\kappa\text{-(ET)}_2\text{Cu}[\text{N}(\text{CN})_2]\text{Br}$  we found that the orbital pairing was not the conventional isotropic  $s$ -wave state. Instead, we concluded that there must be nodes (or near nodes) in the gap, as found in  $d$ -wave or highly anisotropic  $s$ -wave-type pairing states.

In this paper, we report  $^{13}\text{C}$  NMR line position, linewidth, and spin-spin relaxation time  $T_2$  studies in an aligned single crystal ( $\sim 2$  mg) of  $\kappa\text{-(ET)}_2\text{Cu}[\text{N}(\text{CN})_2]\text{Br}$  for a wide temperature range  $2 \leq T \leq 300$  K and use them (see below) to gain further insight into this complex system. We believe it will be helpful to the reader to realize that the work presented in Ref. 1 and the present paper are strongly interrelated. Since Ref. 1 was originally submitted to Physical Review Letters, it had to satisfy length constraints, forcing us to omit significant results. The present paper provides them. We summarize the key results of Ref. 1 below. However, the present paper may be better appreciated if the reader also reads our earlier paper, and indeed also reads our paper on

$^1\text{H}$  NMR in this system.<sup>4</sup> In addition to our results on the superconducting pairing state, other important results of Ref. 1 were measurements of the line position, linewidth, and spin-lattice relaxation time  $T_1$  of the two  $^{13}\text{C}$  nonequivalent sites (see below). These showed that very complicated changes took place as one lowered the temperature from 300 K. Below 150 K, the  $^{13}\text{C}$  lines broadened suddenly. Below 50 K the Knight shift dropped precipitously, the product  $T_1 T$  rose rapidly, and certain differences in the two sites became greater. We argued that the data suggested that over the entire temperature range there were magnetic fluctuations which displayed antiferromagnetic correlations but that they became substantially greater below 150 K. We discussed features of our data which suggested that the transition at 150 K involved a spin-density wave. Unfortunately, there are many features of the complex NMR properties which at this time we do not fully understand. For example, we do not have an explanation for the drop in Knight shift below 50 K. It is reminiscent of the "spin-gap" phenomena in the cuprate superconductors whose origin is one of the current unsolved mysteries of those systems. We are not able to give a detailed description of the postulated spin-density wave.

In the present paper, we present the material we could not include in Ref. 1. We believe it further limits possible explanations, but there is a great deal which still cannot be settled definitively.

The major NMR topics we discuss in the present paper are (1) the angular dependence of the NMR spectrum, and how we use it to assign the NMR lines to the two inequivalent  $^{13}\text{C}$  sites; (2) the NMR linewidth in the superconducting states at low enough magnetic fields to reduce the spin-density-wave line broadening greatly, and what we expect it to be in terms of the superconducting penetration depth; (3) the transverse relaxation time  $T_2$ , and what it tells us about the dynamic of the (spin-wave) transition which occur at 150 K.

The measurements have been performed at 8.3 T in an Oxford superconducting magnet, and at 0.6 T in a Varian electromagnet utilizing a Carr-Purcell sequence (40 spin-echo-train) to enhance the poor signal-to-noise ratio in low

field. The sample holder has been machined from Macor, a carbon-free ceramic. A special two-axis goniometer probe was constructed with which the single crystal could be aligned at any orientation with respect to the applied magnetic field. The line shapes were obtained through the fast-Fourier transformation of either a  $90_x$ - $180_x$  ordinary spin echo, or a blinking Pi free induction decay ( $0$ - $t_{\text{wait}}$ - $90_x$  ADD,  $180_x$ - $t_{\text{wait}}$ - $90_x$  SUB), where  $t_{\text{wait}}$  satisfies  $T_2^* \ll t_{\text{wait}} \ll T_1$ ; typical values are  $t_{\text{wait}} \approx 2$  ms. For  $T_2$  measurements, the echo intensity as a function of the delay time  $\tau/2$  between the  $90$  and  $180$  pulses ( $90$ - $\tau/2$ - $180$ - $\tau/2$ -echo) was measured.

Although the present paper is focused on NMR experimental results, none of this work would be possible without the samples, which are single crystals with  $^{13}\text{C}$  atoms inserted at the two central C positions. The preparation of these samples is a crucial part of the work. It is described in Ref. 5.

## II. IDENTIFICATION OF THE RESONANCE LINES

### A. The crystal structure

The quasi-2D crystal structure of  $\kappa$ -(ET) $_2$ Cu[N(CN) $_2$ ]Br is orthorhombic (axes  $a$ ,  $b$ ,  $c$ ) with conducting cation layers composed of pairs of ET molecules forming the  $a$ - $c$  plane. These conducting layers are spaced at  $\sim 15$  Å intervals along the  $b$  axis, sandwiched between insulating anion layers composed of  $\{\text{Cu}[\text{N}(\text{CN})_2]\text{Br}\}_\infty$  polymeric chains. The orientation of the (ET) $_2$  pairs in the plane above the anion plane is the mirror image (in the  $ac$  plane) of the (ET) $_2$  pairs in the plane below the anion plane. In our sample, the central two carbon atoms of the ET molecule have been labeled with the NMR-active isotope  $^{13}\text{C}$  ( $I=1/2$ , 1.1% nat. abundance) while the rest of the carbon sites remain natural abundance. In the  $\kappa$  phase of ET salts, the ET molecules are paired face-to-face in dimers (Fig. 1 of Ref. 1). The inversion symmetry of the ET molecules is broken as a result of the close pairing in the dimer structure, so that the central two carbon sites are inequivalent. We find this effect in the NMR line shape in that there are two discrete  $^{13}\text{C}$  resonance lines from the two central carbon sites, whereas for a single, isolated ET molecule there would be only one. The dimerization causes the central two carbon sites to feel different local magnetic fields, so that each site has a unique magnetic shift and relaxation rate (a factor of  $\sim 3.5x$  different).

### B. The basic spectrum

In Fig. 1(a), the line shape at 8.9 T at room temperature with  $H\parallel a$  is shown. The two lines resulting from the dimer structure are well resolved, with total shifts equal to  $197 \pm 5$  and  $324 \pm 5$  ppm. In Fig. 1(b), the corresponding line shape with  $H\parallel b$  is shown. For this orientation, there are four lines, two centered at  $\sim 50$  ppm and two at  $\sim 250$  ppm. As the field direction is rotated from  $H\parallel a$  to  $H\parallel b$ , the lower (higher) frequency line splits into two sublines, and has also shifted from 197 (324) down to 50 ppm (250 ppm). This doubling of the lines results from the nuclear dipolar interaction between the two central  $^{13}\text{C}$  sites in a single ET molecule. The dipolar splitting varies as  $1 - 3 \cos^2(\theta)$ , where  $\theta$  is the angle that the applied field  $H$  makes with the vector joining the two carbon nuclei. By happenstance, when  $H\parallel a$ , this factor is nearly zero, so that the splitting vanishes.

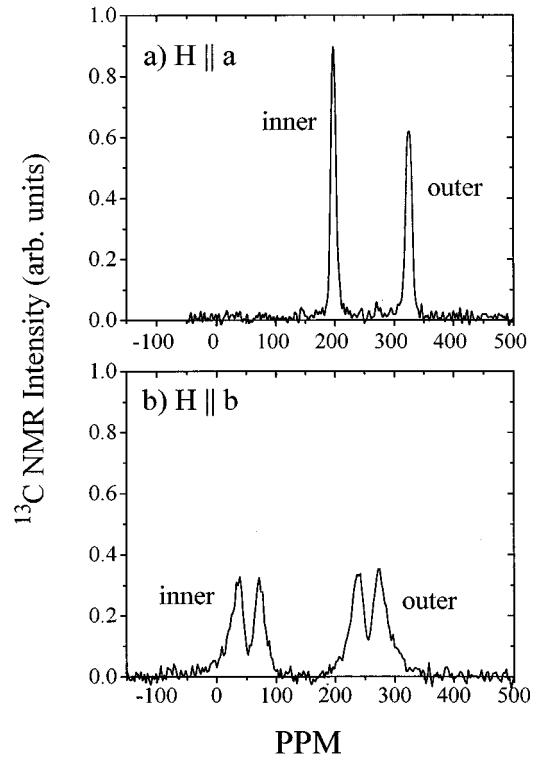


FIG. 1. (a) Room-temperature  $^{13}\text{C}$  NMR line shape with  $H\parallel a$ . (b) Room-temperature line shape with  $H\parallel b$ .

### C. The angular dependence of the NMR lines

To assign each resonance line to the correct site within the dimer, we performed a study of the orientation dependence of the shifts. To do so, we used a goniometer probe capable of rotating the crystal from  $H\parallel b$  to  $H\parallel a$  in  $2.5^\circ$  increments with a resolution of  $0.2^\circ$ . In Fig. 2, we show the measured shifts of the lower and higher frequency resonance lines as a function of  $\theta_{ba}$ , where the magnetic field is constrained to lie in the  $b$ - $a$  plane and  $\theta_{ba}=0^\circ$  corresponds to  $H\parallel b$ . In  $\kappa$ -(ET) $_2$ Cu[N(CN) $_2$ ]Br, the ET molecules are tilted at an angle of  $\sim 36^\circ$  with respect to the  $b$  axis. The sense of this

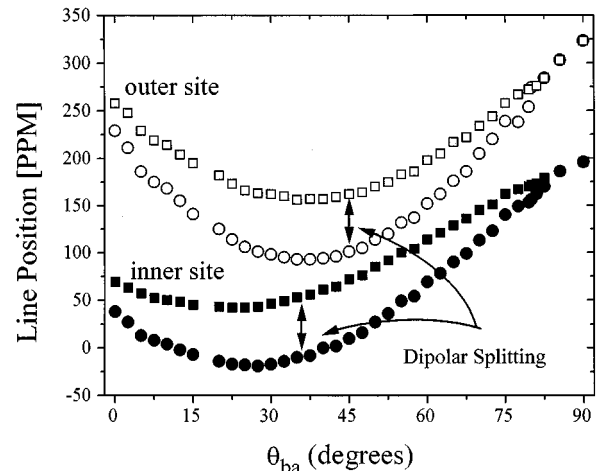


FIG. 2. Angular dependence of  $^{13}\text{C}$  line positions (sum of the magnetic and dipolar shifts) for magnetic fields lying in the  $b$ - $a$  plane.

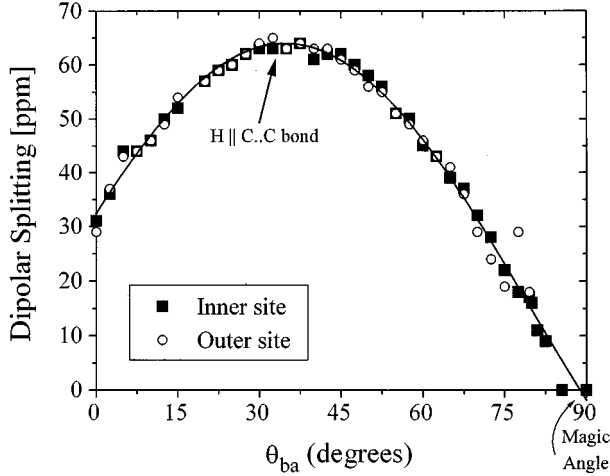


FIG. 3. Angular dependence of  $^{13}\text{C}$  dipolar splitting, obtained by pairwise subtraction in Fig. 1, showing that both sites have the same angular dependence. The angle  $\theta_{ba}=90^\circ$  corresponds to the magic angle. From the fit, we infer that the central carbon-carbon bond length is  $r_{\text{C-C}}=1.39\pm 0.03 \text{ \AA}$ .

tilt in the  $a$ - $b$  plane alternates back and forth between adjacent sets of conducting ET layers. For clarity, and since the information is redundant, we show only the shifts arising from one of the two sets of alternating conducting ET layers. For  $H\parallel a$ , there are only two shifts associated with the line shape of Fig. 1(a). As the magnetic field is rotated away from the  $a$  axis, each line splits into two as a result of the nuclear dipolar coupling between the central two  $^{13}\text{C}$  sites in the same molecule. The squares (circles) are those sites with a spin-down (up) neighbor, and have a corresponding shift in the resonance frequency  $f_{+,-}=f_0\pm f_{\text{dipolar}}$ , where  $f_0$  is the Larmor frequency plus any additional chemical or Knight shifts present. In Fig. 3, we plot the orientation dependence of this dipolar splitting, which is obtained by performing a pairwise subtraction of the shift curves in Fig. 2. The dipolar splitting between two “unlike” spins is given by the following expression:

$$2f_{\text{dipolar}}=f_{+}-f_{-}=\frac{\gamma_n^2 h}{(2\pi)^2}\left(\frac{1-3\cos^2(\theta)}{r^3}\right), \quad (1)$$

where  $r$  is the distance between the spins and  $\theta$  is the angle between the applied field  $H$  and the internuclear vector  $\mathbf{r}$ . From a fit to the data, we determine the distance between the two central carbon atoms,  $r_{\text{cc}}$ , to be  $1.39\pm 0.03 \text{ \AA}$ , which agrees with the value found by an earlier x-ray-diffraction study,  $r_{\text{cc}}=1.37 \text{ \AA}$ .<sup>6</sup> We note that both the sites have the same angular dependence for the dipolar splitting. This is unlike the magnetic shifts at the two sites which we will discuss next.

#### D. Assigning the inner and outer sites

In Fig. 4, the orientation dependence of the magnetic shift has been isolated by pairwise averaging of the shift curves, i.e.,  $(f_{+}+f_{-})/2$ . In this way, the dipolar contribution to the line position has been removed. The most striking aspect of the data shown in the figure is that the shift curves reach their respective extrema  $K_{\text{min}}$  at different values of  $\theta_{ba}$ , unlike the

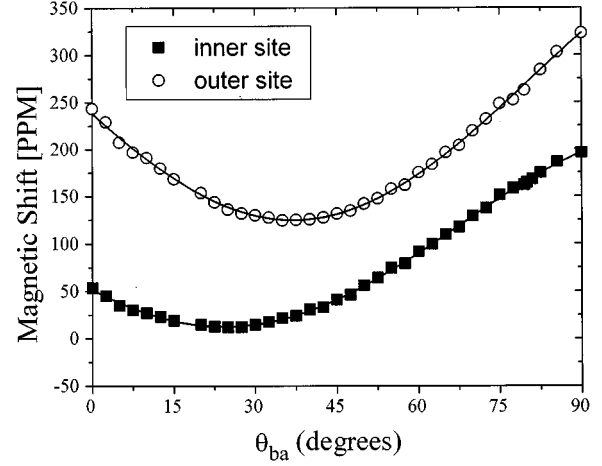


FIG. 4. Angular dependence of magnetic shift, obtained by pairwise averaging in Fig. 1. The sites have maxima at different values of  $\theta_{ba}$ , implying different orientations of principal axes.

dipolar splitting of Fig. 3. This observation indicates that the principal axes of the shift tensors differ in their spatial orientation with respect to the crystal and molecular axes. We have calculated the quantitative principal values and principal axes of the magnetic shift tensors at the two sites by performing a least-squares analysis of the curves in Fig. 4. Here, we note that the principal axes of the ET molecules do not correspond to the crystalline  $a$ ,  $b$ ,  $c$  axes. Since the  $^{13}\text{C}$  shift tensors are expected to have nearly the same principal axes as those of the ET molecule itself, it is useful to define a local molecular axis system. In this reference frame, the  $x$  axis lies along the central C-C double bond of the molecule, the  $y$  axis lies in the plane of the molecule, and the  $z$  axis is normal to the plane of the molecule. In our analysis, we find that the principal axes of the higher frequency resonance line (i.e., the line at 324 ppm in Fig. 1) coincide with the  $x$ ,  $y$ ,  $z$  axes of the ET molecule, but those of the lower frequency resonance line (i.e., the line at 197 ppm in Fig. 1) are rotated about the  $y$  axis of the molecule by  $\sim 6^\circ$ . As explained in Ref. 1, this angular tilt corresponds to the direction of the C-C vector joining the inner C atom of one ET molecule with the inner C atom of the neighboring molecule in a dimer. From this result, we identify the lower (higher) frequency line as the “inner” (“outer”)  $^{13}\text{C}$  site, where the inner (outer) site is closer to (farther from) the center of the dimer.

### III. SUPERCONDUCTING STATE LINEWIDTH

#### A. Fluxoids and how they broaden the NMR line

The NMR linewidth is sensitive to the distribution of local magnetic fields in a sample. In a type-II superconductor in the mixed state ( $H_{c1}<H<H_{c2}$ ), the applied magnetic field penetrates the sample in an array of fluxoids, or quantized tubes of magnetic flux. In conventional type-II superconductors, the fluxoids form a triangular Abrikosov lattice. In some cases (e.g., high-temperature superconductors), vortex glass formation and/or pinning of fluxoids interfere with the long-range order of the lattice. This fluxoid structure will result in variations of the local magnetic-field intensity, with

maxima in the fluxoid cores, and minima at the center of three neighboring fluxoids. The parameter describing the length scale over which the field drops off is the magnetic penetration depth,  $\lambda(T)$ . The penetration depth, together with the fluxoid spacing distance, determines the total variation in the internal magnetic field in the mixed state.

The density of fluxoids per unit area  $n$  is proportional to the applied magnetic field:  $H = n\Phi_0$ , where  $\Phi_0 = 2 \times 10^{-7}$  G cm<sup>2</sup> is the magnetic flux quantum. Using this relation, we find that the spacing between fluxoids is on the order of  $d \sim 500$  Å in a field of 0.5 T, while in a larger applied field of 8.3 T, the vortex-vortex distance is reduced to  $d \sim 150$  Å. The zero temperature in-plane London magnetic penetration depth for  $\kappa$ -(ET)<sub>2</sub>Cu[N(CN)<sub>2</sub>]Br has been estimated to be  $\lambda_{ac}(T=0) = 6500$  Å,<sup>7</sup> so that there should be a measurable ripple of the field intensity between the fluxoids. In a layered superconductor, such as  $\kappa$ -(ET)<sub>2</sub>Cu[N(CN)<sub>2</sub>]Br, the penetration depth depends on the orientation of the applied field with respect to the layers. When the field is applied perpendicular to the conducting planes ( $H \perp a$ -c), only the in-plane screening currents come into play. For  $H \parallel a$ -c, however, both the in-plane and the inter-layer screening currents are required. We can define effective penetration depths for the two cases as follows:

$$\lambda_{\text{eff}}^{\perp} = \lambda_{\text{in-plane}} \quad \text{for } H \perp a\text{-c}, \quad (2a)$$

$$\lambda_{\text{eff}}^{\parallel} = (\lambda_{\text{in-plane}} \times \lambda_{\perp \text{plane}})^{1/2} \quad \text{for } H \parallel a\text{-c}, \quad (2b)$$

where

$$\lambda_{\text{in-plane}} < \lambda_{\perp \text{plane}}, \quad (2c)$$

since the in-plane current is larger than the interlayer current, which involves the weak Josephson coupling between layers. The situation  $H \perp a$ -c is cleaner experimentally since it involves only  $\lambda_{\text{in-plane}}$ . Finally, we remark that the crystallographic unit-cell dimensions are on the order of 10 Å, which is much smaller than the intervortex spacing ( $\sim 500$  Å). This implies that the <sup>13</sup>C nuclei under study should be on a fine enough grid to probe the variations of the local magnetic field. The NMR line shape should then be a direct mapping of the distribution of local magnetic fields produced by the fluxoid system.

### B. The NMR line shapes at low field

A series of <sup>13</sup>C line shapes taken below  $T_c$  with  $H \parallel a$ ,  $H = 0.5$  T is shown in Fig. 5. At this low field, the line broadening observed at 8.3 T below 150 K is absent. The <sup>13</sup>C resonance line is quite narrow ( $\sim 2$  G) at  $T_c$ , and then broadens below  $T_c$  due to inhomogeneities of the internal magnetic field associated with the formation of the fluxoid lattice. The additional broadening in the superconducting state was only observed in the weakest applied field (0.6 T). In high fields (e.g.,  $H = 8.3$  T), the line is already very broad at  $T_c$  as a result of the spin-density-wave transition at 150 K and no additional broadening may be observed below  $T_c$ . For applied fields  $H$  between  $H_{c1}$  and  $H_{c2}$ , it has been shown<sup>8</sup> that the fluxoid contribution to the second moment of the NMR line shape is independent of the size of the applied field. In  $\kappa$ -(ET)<sub>2</sub>Cu[N(CN)<sub>2</sub>]Br, estimates for the lower and

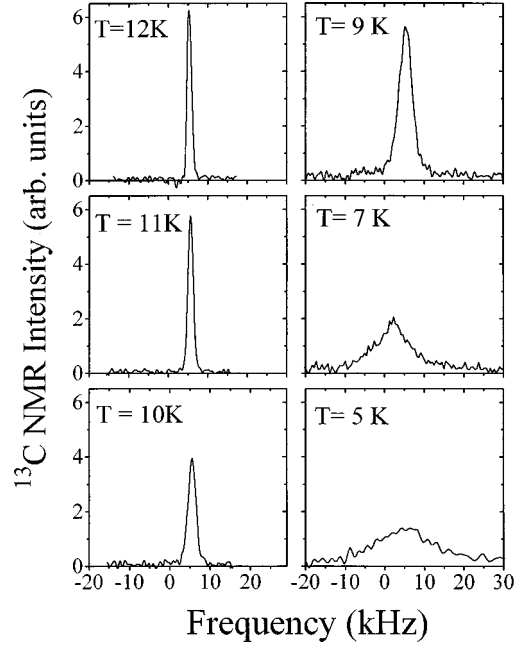


FIG. 5. Sequence of low-field line shapes for  $T < T_c = 11.6$  K for  $H \parallel a$ , showing the broadening due to the fluxoid lattice.

upper critical fields are  $H_{c1} \approx 20$  G and  $H_{c2} \approx 216$  T.<sup>7,9</sup> The field used here,  $H = 0.6$  T (6000 G), is clearly in this intermediate regime. In this limit, the theoretical fluxoid contribution to the second moment of the NMR line resulting from the vortex lattice is

$$\sqrt{\langle \Delta H^2 \rangle} \cong \frac{\Phi_0}{\lambda^2 \sqrt{16\pi^3}}. \quad (3)$$

The <sup>13</sup>C NMR second moment measured below  $T_c$  has contributions from both the fluxoid lattice and normal-state broadening mechanisms (dipolar, field inhomogeneity, etc.) In the limit of a Gaussian line shape, the second moment may be directly related to the linewidth, as measured by the full width at half maximum (FWHM). In order to get quantitative measurements of the second moment of our line shapes, we have approximated the <sup>13</sup>C line shapes as Gaussian, and estimated second moments from the measured FWHM linewidth. In making this approximation, we realize that the penetration depths we shall derive may have small systematic errors. To remove the normal-state contribution to the linewidth,  $\langle \Delta H^2 \rangle_{\text{ns}} \approx 1$  G<sup>2</sup>, we use the following procedure:

$$\sqrt{\langle \Delta H^2 \rangle}_{\text{fluxoid}} = (\langle \Delta H^2 \rangle_{\text{measured}} - \langle \Delta H^2 \rangle_{\text{ns}})^{1/2}, \quad (4)$$

where all quantities are defined as FWHM linewidths.

### C. The temperature dependence of the linewidth

In Fig. 6, we show the temperature dependence of the linewidth for a magnetic field perpendicular to the conducting layers in a weak applied field,  $H = 0.6$  T with  $H \perp a$ -c (line shapes not shown). If one has an independent estimate for  $\lambda_{ac}(T)$ , then the expected NMR linewidth  $\sqrt{\langle \Delta H^2 \rangle}_{\text{fluxoid}}$  can be calculated via Eq. (3). Lang *et al.* have measured

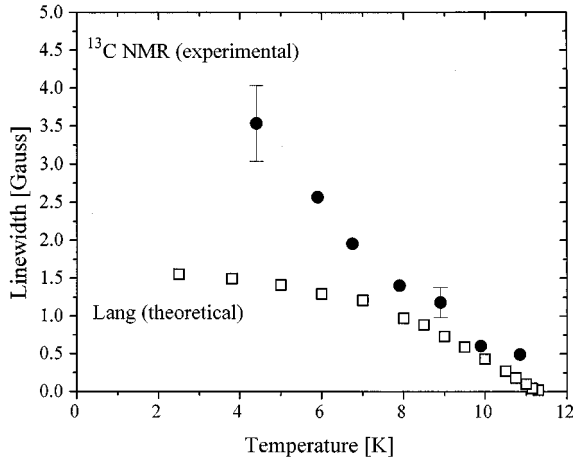


FIG. 6. Temperature dependence of the low-field  $^{13}\text{C}$  NMR FWHM linewidth for  $H\perp ac$  compared with implied theoretical values using Eq. (3) and the reversible magnetization data by Lang.

$\lambda_{ac}(T)$  by measuring the magnetization as a function of applied field ( $H\perp a-c$ ) in the reversible regime.<sup>7</sup> In Fig. 6, we show the NMR linewidths one would expect using the Lang values of  $\lambda_{ac}(T)$  and Eq. (3). Their data are well described by the conventional BCS model, with a linear rise of the linewidth just below  $T_c$  and then saturating behavior at lower temperatures. In contrast, the NMR linewidth increases linearly as the temperature is lowered below the superconducting transition, with no evidence of a flattening out tendency down to the lowest temperatures measured. In Ref. 1, we conclude that the spin-lattice relaxation rate ( $1/T_1$ ) data require that  $\kappa\text{-(ET)}_2\text{Cu}[\text{N}(\text{CN})_2]\text{Br}$  be an unconventional superconductor with a line of nodes or near nodes in the energy gap. If this is the case, then as discussed by Hardy *et al.*,<sup>10</sup> at low temperatures  $1/\lambda^2$  will obey a power law:

$$\sqrt{\langle \Delta H^2 \rangle}_{\text{fluxoid}} \sim \frac{\lambda^2(0)}{\lambda^2(T)} = 1 - bT, \quad (5)$$

where  $b$  is a positive constant. The linewidth data of Fig. 6 are consistent with such a situation, and are reminiscent of the plot of  $\lambda^2(0)/\lambda^2(T)$  in Fig. 4 of Hardy *et al.* Thus, the linewidth data with  $H\perp a-c$  are consistent with the conclusion of our  $T_1$  data that our sample is an unconventional superconductor, perhaps with a line of nodes.

#### D. Fluxoid motion— $^1\text{H}$ versus $^{13}\text{C}$

From our  $^1\text{H}$   $T_1$  measurements,<sup>1</sup> we know that fluxoid motion is responsible for the spin-lattice relaxation time of the protons, which interact very weakly with the conduction electron spin fluctuations due to their position within the ET molecule. If the fluxoid motion implied from the  $^1\text{H}$  results were large scale, the  $^{13}\text{C}$  would experience motional narrowing and Eq. (3) above would no longer apply. This situation has been reported by Pennington *et al.* for  $^{63}\text{Cu}$  in  $\text{YBa}_2\text{Cu}_3\text{O}_{7-x}$  just below  $T_c$  in the so-called “fluxoid liquid” regime. At lower temperatures, as the fluxoids become immobile in the “fluxoid glass” regime, they observe a line broadening, which grows as the temperature is lowered, similar to Fig. 6.

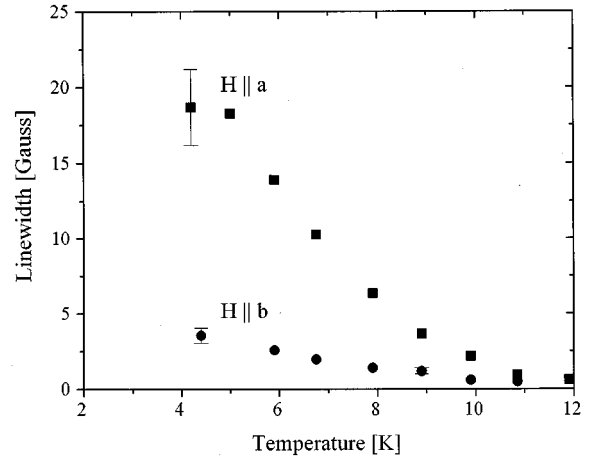


FIG. 7. Temperature dependence of the low-field  $^{13}\text{C}$  NMR linewidth for  $H\parallel b$  (circles) and  $H\parallel a$  (squares).

We can reconcile the  $^1\text{H}$  and  $^{13}\text{C}$  results in  $\kappa\text{-(ET)}_2\text{Cu}[\text{N}(\text{CN})_2]\text{Br}$  if we assume that the fluxoid motions are small in scale relative to the distance between fluxoids, i.e., small vibrations about equilibrium positions. In this way, the fluxoids can relax the protons, but do not motionally narrow the  $^{13}\text{C}$  NMR line. In this picture, the protons near a vortex experience rapid spin-lattice relaxation from the large field fluctuations, while those protons further away are relaxed through a process of spin diffusion. We found that the recovery of the  $^1\text{H}$  magnetization in a saturation recovery experiment was not a single exponential in time, which also points to such a model.<sup>11</sup>

#### E. Static field orientation effects

In Fig. 7, we show the low-field ( $H=0.6$  T)  $^{13}\text{C}$  linewidths below  $T_c$  for  $H\parallel a$  (measured from the line shapes in Fig. 5) together with the data for  $H\perp a-c$  already shown in Fig. 6. From Eqs. (2) and (3) we expect the linewidth to be narrower for  $H\parallel a$  (parallel to the layers). However, the observed linewidths are much larger for  $H\parallel a$ , indicating greater inhomogeneities of the local magnetic field when the fluxoids are parallel to the layers than when they are perpendicular. Quite similar behavior has been found in  $^{63}\text{Cu}$  NMR in  $\text{YBa}_2\text{Cu}_3\text{O}_{7-x}$ . Barrett *et al.* found that there was an additional broadening in the superconducting state, perhaps separate from that due to the fluxoid system. Just as in  $\kappa\text{-(ET)}_2\text{Cu}[\text{N}(\text{CN})_2]\text{Br}$ , the broadening was much larger for fields parallel to the layers ( $H\perp c$ ) than for fields perpendicular ( $H\parallel c$ ). The broadening was not well understood, although it was presumed to arise from localized impurity spins, due to its Curie-Weiss temperature dependence.

Other studies of the magnetic penetration depth have found evidence for unconventional superconductivity in  $\kappa\text{-(ET)}_2\text{Cu}[\text{N}(\text{CN})_2]\text{Br}$ . Takahashi, Kanoda, and Saito measured the complex susceptibility and found no evidence for saturating behavior in  $1/\lambda^2(T)$  at low  $T$ .<sup>12</sup> Le *et al.* found a linear variation of  $\lambda$  at low temperatures in their muon-spin-relaxation ( $\mu\text{SR}$ ) studies of  $\kappa\text{-(ET)}_2\text{Cu}[\text{N}(\text{CN})_2]\text{Br}$ .<sup>13</sup>

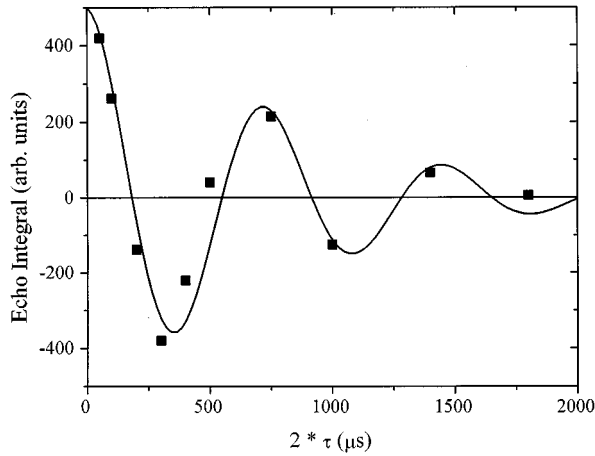


FIG. 8. Spin-spin relaxation ( $T_2$ ) recovery at room temperature with  $H\parallel b$ .

#### IV. TRANSVERSE RELAXATION ( $T_2$ )

##### A. Room temperature

We have measured the decay of the spin-echo envelope, or the so-called transverse or spin-spin relaxation ( $T_2$ ) decay curve, at room temperature. In this case, the spin-spin relaxation results from both  $^{13}\text{C}$ - $^{13}\text{C}$  and  $^{13}\text{C}$ - $^1\text{H}$  dipolar interactions. The central two carbon atoms within a single ET molecule are very strongly coupled and, in fact, form singlet and triplet spin states, as reflected in their spin-lattice relaxation and line intensity characteristics. This coupling results in a modulation of the  $T_2$  decay curve,  $\cos(a_{io}\tau)$ , where  $a_{io}$  is the strength of the dipolar coupling between the inner and outer  $^{13}\text{C}$  sites. The coupling to the other  $^{13}\text{C}$  nuclei in neighboring ET molecules results in an additional term in the spin-spin decay curve, which we approximate as a Gaussian, with time constant  $T_{2G}$  chosen to match the theoretical second moment calculations. Lastly, the coupling to the thermally fluctuating  $^1\text{H}$  spins in the ethylene groups on the ends of the molecules produces an extra exponential term in the relaxation, so that the observed relaxation for nucleus is given by

$$M(\tau) = e^{-1/2(\tau/T_{2G})^2} e^{-\tau/T_2} \cos(a_{io}\tau), \quad (6)$$

where  $\tau$  is the time span between the initial  $\pi/2$  pulse and the center of the spin echo. In Fig. 8, we display our data at 8.3 T for  $H\parallel b$  at  $T=292$  K together with the theoretical decay of Eq. (6). The constant  $a_{io}$  is determined by the crystal structure, and the best fit has been found using an exponential  $T_2 = 1200(\pm 300)\mu\text{s}$ .

##### B. Extra transverse relaxation near the 150 K transition

Previously, we reported that a  $^{13}\text{C}$  line broadening transition occurs at 150 K in a large applied magnetic field (8.3 T).<sup>1</sup> This transition is also reflected in changes of the Knight shift and spin-lattice relaxation rate ( $1/T_1$ ). In an effort to further our understanding of this transition, we report in this paper the effect of this transition on the transverse relaxation rate ( $1/T_2$ ).

Above 150 K, for  $H\parallel a$ , the  $^{13}\text{C}$  lines are quite sharp, and the experimental linewidth of  $\sim 10$  ppm at both the inner and

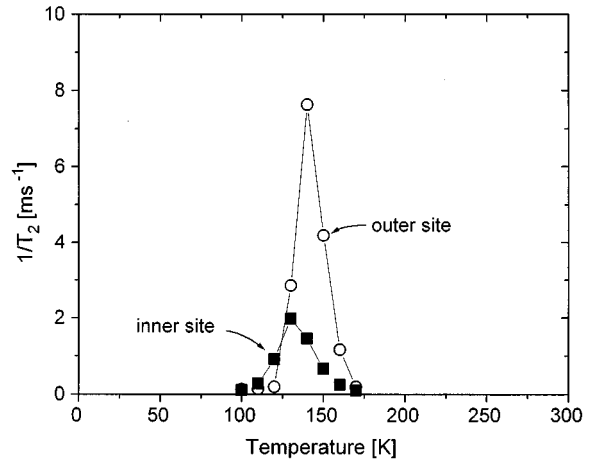


FIG. 9. Temperature dependence of extra exponential component of spin-spin relaxation for  $H\parallel a$ .

outer sites may be accounted for by the  $^{13}\text{C}$ - $^{13}\text{C}$  dipolar couplings (Fig. 1). The measured  $^{13}\text{C}$  linewidth is constant down to about 150 K, below which there is a dramatic broadening, with the linewidth increasing from 10 to 60 ppm for the outer site as the crystal is cooled from 150 to 125 K.<sup>1</sup> The inner site linewidth also increases, although to not as great a degree as that of the outer site. The excess broadening remains below 100 K, even down into the superconducting state.

The NMR linewidth quantifies the static distribution in the longitudinal ( $z$  axis) local magnetic fields throughout the crystal. The exponential component of the transverse relaxation rate  $1/T_2$ , on the other hand, is affected by quasistatic fluctuations of the local longitudinal magnetic fields. If the local field at an individual nucleus changes during the  $90^\circ$ - $\tau/2$ - $180^\circ$ -echo pulse sequence, then the nuclear spin will not refocus perfectly with the other spins in the sample at the time  $\tau$ , resulting in a decrease of the echo intensity. If the fluctuations are random, as for case of the fluctuating fields produced by the motion of the ethylene group protons, the decay of the echo intensity will be exponential, yielding a spin-spin relaxation time  $T_2$ :

$$M(\tau) = M_0 e^{-\tau/T_2}. \quad (7)$$

As seen above, the room temperature  $T_2$  decay curve in  $\kappa$ -(ET)<sub>2</sub>Cu[N(CN)<sub>2</sub>]Br is well described by spin-spin interactions. However, in the range  $110\text{K} < T < 160$  K, the experimental  $T_2$  decay curve becomes more pronounced and an additional term is needed to fit the data. This additional  $T_2$  component results from the same fluctuations that produce the line broadening transition in this temperature range. Although the  $T_2$  data are not perfectly described by a single exponential, we use such a fit to provide a quantitative picture of the temperature dependence of this extra spin-spin relaxation, shown in Fig. 9. The rate increases from zero above 175 K, reaches a maximum at a temperature of 135 K (125 K) for the outer (inner) site, and then drops sharply to zero once again. The data indicate that fluctuations of the local longitudinal field appear below 170 K, which are also reflected in the static linewidth measurements. The fluctuations reach a maximum amplitude at slightly different temperatures for the two sites, and then freeze out below 110 K.

As the sample is cooled below this temperature, spatial variations of the local longitudinal magnetic fields still persist, as reflected in the continued excess static line broadening. However, these variations are fixed in time and the longitudinal field at a given nucleus does not vary on the time scale of the spin-echo experiment ( $\tau \sim 1$  ms), as evidenced by the vanishing of the extra spin-spin relaxation contribution.

The situation can be expressed semiquantitatively by considering a model in which the nuclear precession frequency jumps between values  $\pm \delta\omega$  with a correlation time  $\tau$ . When  $\tau$  is long ( $|\delta\omega\tau| \gg 1$ ), one has the case of strong collisions with  $T_2 = \tau$ . When  $\tau$  is short [ $(\delta\omega\tau)^2 \ll 1$ ] one has motional narrowing; then  $1/T_2 = (\delta\omega)^2\tau$ . These two cases can be encompassed by the formula

$$\frac{1}{T_2} = \frac{\delta\omega^2\tau}{1 + (\delta\omega\tau)^2}, \quad (8)$$

which describes our data if we consider  $(\delta\omega)$  to represent the line broadening and  $\tau$  correlation time of the fluctuations. Evidently  $\delta\omega$  is somewhat a function of temperature (particularly just below 150 K where the line breadth grows rapidly as the temperature drops).

If  $\delta\omega$  were independent of temperature, the peak in  $1/T_2$  occurs when  $\delta\omega\tau = 1$ , and at the peak  $T_2 = 2\tau$ . We can thus estimate that at 125 K,  $\tau \cong 250 \mu\text{s}$ , and at 135 K it is about  $65 \mu\text{s}$ . We can see from Eq. (8) that the reason the outer site peaks at a higher temperature is because its NMR line is broader.

In our earlier paper, we showed that AF fluctuations were responsible for the temperature dependence of the spin-

lattice relaxation rate and the Knight shift as measured by the Pines correction to the Korringa factor. We postulated that the transition at 150 K was therefore a spin-density-wave transition. The present results incorporating both the static linewidth and dynamic spin-spin relaxation rate give further support to this model of the transition.

## V. CONCLUSIONS

In conclusion, we have identified which NMR lines belong to the inner site and which to the outer site. We have shown that in the superconducting state when  $H$  is perpendicular to the conducting planes, the NMR linewidth is consistent with broadening by fluxoids and with unconventional pairing, but that there appears to be an extra broadening mechanism when  $H$  lies in the conducting planes. Lastly, by  $T_2$  measurements we have measured the time scale of magnetic fluctuations at temperatures just below the onset of the linewidth transition at 150 K.

## ACKNOWLEDGMENTS

The authors thank T. Imai, R. Corey, N. Curro, C. Milling, D. Smith, V. Barzykin, A. Sokol, and D. Pines for helpful discussions related to this work. This research has been supported through the University of Illinois Materials Research Laboratory by a grant from the DOE Division of Materials Research under Grant No. DEFG02-91ER45439 (S.M.D., C.P.S.) and the Science and Technology Center for Superconductivity under Grant No. DMR 88-09854 (C.P.S.) and through Argonne National Laboratory by the DOE Division of Material Science under Contract No. W-31-109-ENG-38 (A.M.K., H.H.W., U.G., J.M.W.).

<sup>1</sup>S. M. DeSoto *et al.*, Phys. Rev. B **52**, 10 364 (1995).

<sup>2</sup>H. Mayaffre *et al.*, Europhys. Lett. **28**, 205 (1994).

<sup>3</sup>A. Kawamoto *et al.*, Phys. Rev. Lett. **74**, 3455 (1995).

<sup>4</sup>S. M. DeSoto, C. P. Slichter, H. M. Want, U. Geiser, and J. M. Williams, Phys. Rev. Lett. **70**, 2956 (1993).

<sup>5</sup>K. D. Carlson *et al.*, Inorg. Chem. **31**, 3346 (1992); A. M. Kini *et al.*, *ibid.* **29**, 2555 (1990).

<sup>6</sup>U. Geiser *et al.*, Acta Crystallogr. C **47**, 190 (1991).

<sup>7</sup>M. Lang *et al.*, Phys. Rev. B **46**, 5822 (1992).

<sup>8</sup>P. Pincus *et al.*, Phys. Lett. **13**, 21 (1964).

<sup>9</sup>W. K. Kwok *et al.*, Phys. Rev. B **42**, 8686 (1990).

<sup>10</sup>W. Hardy *et al.*, Phys. Rev. Lett. **68**, 1923 (1992).

<sup>11</sup>Recently Mayaffre *et al.* have published a <sup>1</sup>H NMR study of fluxoid dynamics: H. Mayaffre, P. Wzletek, D. Jerome, and S. Bazovskii, Phys. Rev. Lett. **76**, 4951 (1996).

<sup>12</sup>T. Takahashi, K. Kanoda, and G. Saito, Physica C **185-189**, 366 (1991).

<sup>13</sup>L. P. Le *et al.*, Phys. Rev. Lett. **68**, 1923 (1992).